Pulsed Laser Activation Method for Hydrogen Storage Alloys

Bruno Hessel Silva[1], Juliana M. P. Almeida[1], Antonio C Hernandes[2], Renato V. Gonçalves[2], Guilherme Zepon[1,3,*]

[1] Federal University of São Carlos, Department of Materials Engineering (DEMa/UFSCar) – Rod. Washington Luiz, km 235, São Carlos – São Paulo, Brasil CEP:13565-905.

[2] São Carlos Institute of Physics, University of São Paulo, PO Box 369, 13560-970, São Carlos, SP, Brazil.

[3] Federal University of São Carlos, Graduate Program in Materials Science and Engineering (PPGCEM/UFSCar) – Rod. Washington Luiz, km 235, São Carlos – São Paulo, Brazil CEP:13565-905.

* Corresponding author: zepon@ufscar.br

Abstract

The activation procedures of metals and alloys for hydrogen absorption might be a considerable challenge for large-scale applications of metal hydrides. In this work, the Pulsed Laser Activation (PLA) method for hydrogen storage alloys is introduced for the first time. We show that the hydrogen storage ability of an aged (air-exposed for 30 days) $Ti_{11}V_{30}Nb_{28}Cr_{31}$ body-centered cubic alloy is restored by scanning the sample with a nanosecond pulsed laser for only three minutes. X-Ray Diffraction (XRD), Scanning Electron Microscopy (SEM) and X-ray Photoelectron Spectroscopy (XPS) analyses were performed to investigate structural features that changed in the $Ti_{11}V_{30}Nb_{28}Cr_{31}$ samples after ageing and after the PLA treatment. Surface remelting, oxide layers and crack formation seem to be factors that affect the hydrogen storage ability of the $Ti_{11}V_{30}Nb_{28}Cr_{31}$ alloy activated via PLA. Although the mechanisms involved in the PLA are not clear yet, this procedure opens a new path for the development of activation methods based on laser-metal interactions which can be easily applied in alloys and metals for hydrogen storage systems.

1. Introduction

Green hydrogen as a vector to store and transport energy from renewable and sustainable sources has a central role in the fight against climate changes. However, the storage and transport of large amounts of hydrogen gas is a bottleneck to the widespread use of hydrogen as an energy vector. Metal hydrides have been studied for more than fifty years for solid-state hydrogen storage. In addition to have high volumetric hydrogen storage capacities (for instance, 150 kg H_2 / m³ for the Mg_2FeH_6 and 115 kg H_2 / m³ for the $LaNi_5H_6$ [1]), the metal hydrides hydrogen storage properties can be tuned by composition control. In the past few years, many alloys and intermetallic compounds with a large range of hydrogen storage properties have been developed [2–16]. Multicomponent alloys with body-centered cubic (BCC) structure, such as TiVZrNbHf [3,8], TiZrNbHfTa [5], and TiVNbCr [6,13,17,18], have been calling the attention because they can absorb up to 2 H/M (hydrogen to metal atoms ratio) with fast kinetics by forming a face-centered cubic (FCC) hydride. This behavior is similar to the traditional ternary BCC alloys, such as those of the Ti-V-Cr system [19–24]. However, by adding or substituting other alloying elements the thermodynamic properties of the metal-hydrogen system can be tuned and, therefore, the pressure-temperature conditions for hydrogen absorption/desorption adjusted for different applications.

Recently, we reported the development of a new BCC alloy, namely, $Ti_{11}V_{30}Nb_{28}Cr_{31}$, with room-temperature hydrogen absorption/desorption reversibility [25]. This alloy can absorb up to 2.5 %wt. of H in a few minutes under mild hydrogen pressure (below 25 bar) and 25 °C, which can be desorbed by simply reducing the system pressure to 1 bar. It was shown that if this alloy is exposed to air for 30 days, its hydrogen absorption is inhibited. In most of the transition metals and alloys, surface states impermeable to hydrogen are formed on exposure to air. Only after activation treatment, i.e., heating the specimen to some specific temperature under dynamic vacuum or H_2 gas, the surface becomes permeable to hydrogen. Indeed, the $Ti_{11}V_{30}Nb_{28}Cr_{31}$ alloy restored its absorption capacity when the air-exposed sample was heated at 400 °C under dynamic vacuum for 3 hours [25].

Although many alloys with promising hydrogen storage properties have been investigated, only few of the recent works focus on their activation procedures [26–28]. While for lab-scale experiments the activation treatment represents no burden, it can be very unpractical for large-scale tanks and applications. In this context, finding new activation procedures that avoid long heat treatments under vacuum or under high

pressure conditions might be paramount for metal hydrides applications. Therefore, in the present work, we decided to explore a novel activation method for hydrogen storage alloys based on nanosecond pulsed laser technique, namely Pulsed Laser Activation (PLA). This PLA method is based on the Laser-direct writing technique, which is mainly employed in transparent amorphous material, as glasses and polymers, with applications in 3D optical waveguides [29–32] or even in transparent crystalline solids, as for defect engineering in diamond [33]. Herein, we take advantage of the fact that laser-metal interactions occur only superficially, and we investigate the effect of PLA on the hydrogen storage behavior of air-exposed $Ti_{11}V_{30}Nb_{28}Cr_{31}$ alloy.

2. Materials and methods

2.1. Alloy synthesis and PLA procedure

The $Ti_{11}V_{30}Nb_{28}Cr_{31}$ alloy was produced via arc melting under argon atmosphere using high purity elements (purity higher than 99.5%). Ti-getter pieces were melted in the furnace prior to each fusion to minimize oxygen contamination in the samples. The ingot was remelted ten times being turned upside down between each remelt step to improve chemical homogeneity. Subsequently, the alloy was stored and handled in a MBRAUM glovebox under argon atmosphere with levels of O_2 and H_2O lower than 0.5 ppm. Small samples were removed from the ingot and analyzed in three different conditions: 1) Pristine sample, crushed using a stainless-steel mortar and pestle inside the glovebox avoiding air-exposure prior to the analyses; 2) Aged sample, which was removed from the glovebox, crushed, and left exposed to air for 30 days with room temperature varying between 21-23 ºC and humidity levels varying between 50-70%; and 3) Pulsed Laser-activated (PLA) sample, which corresponded to a portion of the aged sample subjected to the PLA technique hereafter referred to as aged+PLA sample.

The aged+PLA sample was obtained by spreading 0.5 g of aged $Ti_{11}V_{30}Nb_{28}Cr_{31}$ alloy in a stage of 12 mm x 16 mm area that was subjected to a nanosecond pulsed laser scanning the fragments with a constant speed of 400 mm/min. The whole area was scanned 4 times, resulting in a processing time of ~ 3 min. The experimental setup was composed of a Nd:YAG laser (pulses of 10 ns, at 1064 nm, repetition rate of 10 Hz, operating with 0.8W of average power), a focusing lens (f = 15 cm) and a computer controlled x-y translational stages, as illustrated in Figures 1 (a) and (b).

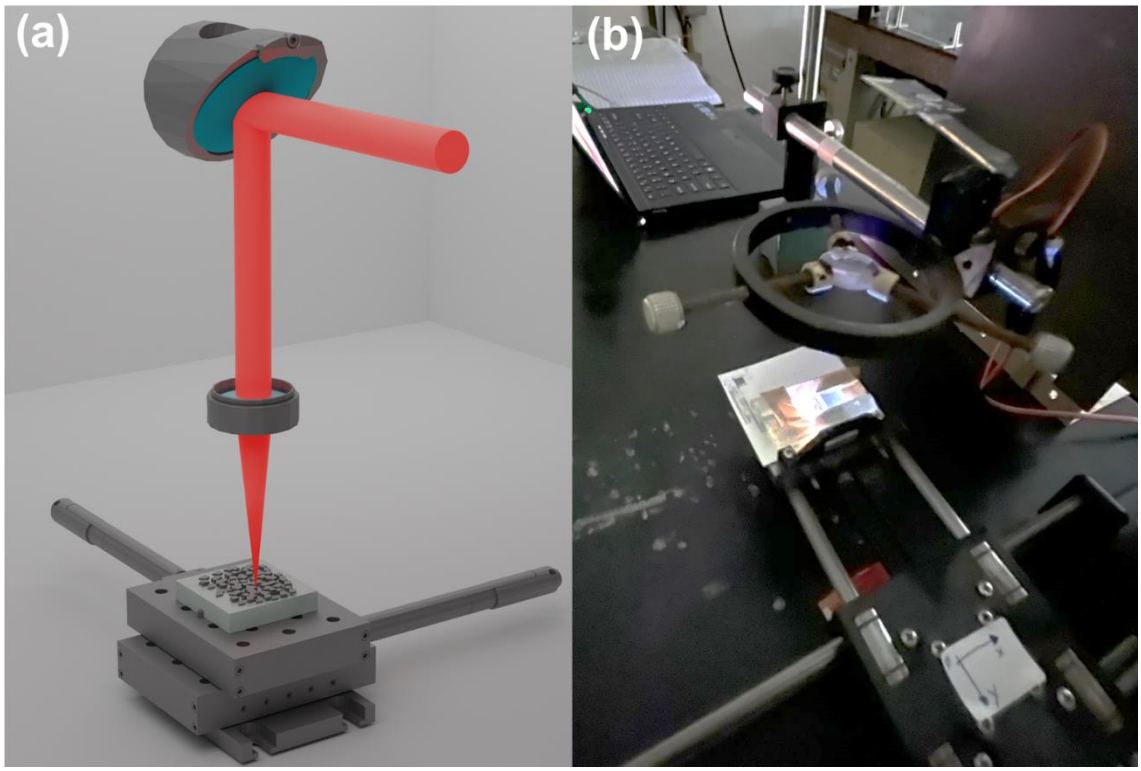

Figure 1: a) Illustration and b) picture of the experimental setup for Pulsed Laser Activation. The fragmented alloy is placed in x-y translation stage, which moves the sample concerning the focused laser beam at constant speed.

2.2. Sieverts analyses and structural characterizations

Hydrogen absorption kinetics of the $Ti_{11}V_{30}Nb_{28}Cr_{31}$ alloy was evaluated for the three conditions mentioned in section 2.1 (pristine, aged and aged+PLA). These measurements were performed in a PCT-Pro SETARAM Sieverts-type apparatus using fragmented samples at room-temperature (25 °C) and 25 bar of initial hydrogen pressure. X-Ray Diffraction (XRD) analyses were performed in samples before and after hydrogenation using a D8 Advance ECO Bruker diffractometer with Cu-Kα radiation. Scanning Electron Microscopy (SEM) analyses were carried out in a XL30 Philips FEG microscope collecting Secondary Electrons (SE) images of the pristine and aged+PLA samples before and after hydrogenation. The surface electronic structure of the samples was probed using X-ray photoelectron spectroscopy (XPS). The analysis was conducted using a Scienta Omicron ESCA+ instrument with an Al Kα source, and a low-energy electron flood gun was used for charge compensation. A pass energy of 30 eV was applied

with energy increments of 0.05 eV for high-resolution spectra. The binding energy of adventitious carbon (C-C/C-H bonds at 284.8 eV) served as the reference point for XPS spectra calibration. Data analysis was carried out using CasaXPS software.

3. Results and discussions

To identify possible phase transitions due to ageing and/or PLA treatment, XRD analyses were performed in the pristine, aged, and aged+PLA samples of the $Ti_{11}V_{30}Nb_{28}Cr_{31}$ alloy as exhibited in Figure 2 (a). The patterns show that the crystalline structure of the pristine alloy – composed of a major BCC phase (with lattice parameter a = 3.113 (1) Å) and a minor fraction of C15-type laves phase (with a = 7.082 (1) Å) [25] – presents no significant change after ageing and PLA treatment. It is worth mentioning that the microstructure of the as-cast $Ti_{11}V_{30}Nb_{28}Cr_{31}$ alloy was comprehensively described elsewhere [25]. Despite no significant changes in their phase structures, the hydrogen storage behavior of the three samples demonstrated substantial differences. Figure 2 (b) shows the kinetics curves of the pristine, aged, and aged+PLA samples. The pristine sample presented a short incubation time followed by a fast absorption process reaching a maximum capacity of ~1.6 H/M (~2.5 wt.%) in less than five minutes. On the other hand, the aged sample did not present any significant amount of hydrogen absorbed even after several minutes. This difference shows how the aging conditions severely affects the hydrogen storage ability of the $Ti_{11}V_{30}Nb_{28}Cr_{31}$ alloy. However, by subjecting the aged sample to the PLA treatment, the aged+PLA sample displayed a hydrogen absorption capacity similar to the pristine sample. Additionally, it is worth mentioning that during the transportation of the sample from the Laser equipment to the Sieverts apparatus (which took approximately 2 hours), the sample was handled on air. Therefore, these results reveal that the PLA method (which took only 3 min of laser scanning) was able to restore the hydrogen storage ability of the air-exposed BCC alloy. Moreover, XRD patterns of the hydrogenated pristine and aged+PLA alloy (Figure 2 (c)) confirmed that both samples presented roughly the same amounts of FCC+BCC+C15 hydride phases indicating similar hydrogenation behavior. The low concentration of FCC hydrides of the hydrogenated samples is associated to the hydrogen desorption reversibility of the $Ti_{11}V_{30}Nb_{28}Cr_{31}$ alloy at room temperature. The reader is referred to [25] for a detailed description of the hydrogenation behavior of Ti-V-Nb-Cr alloys and the thermodynamics aspects behind the FCC hydride stability in the $Ti_{11}V_{30}Nb_{28}Cr_{31}$ alloy.

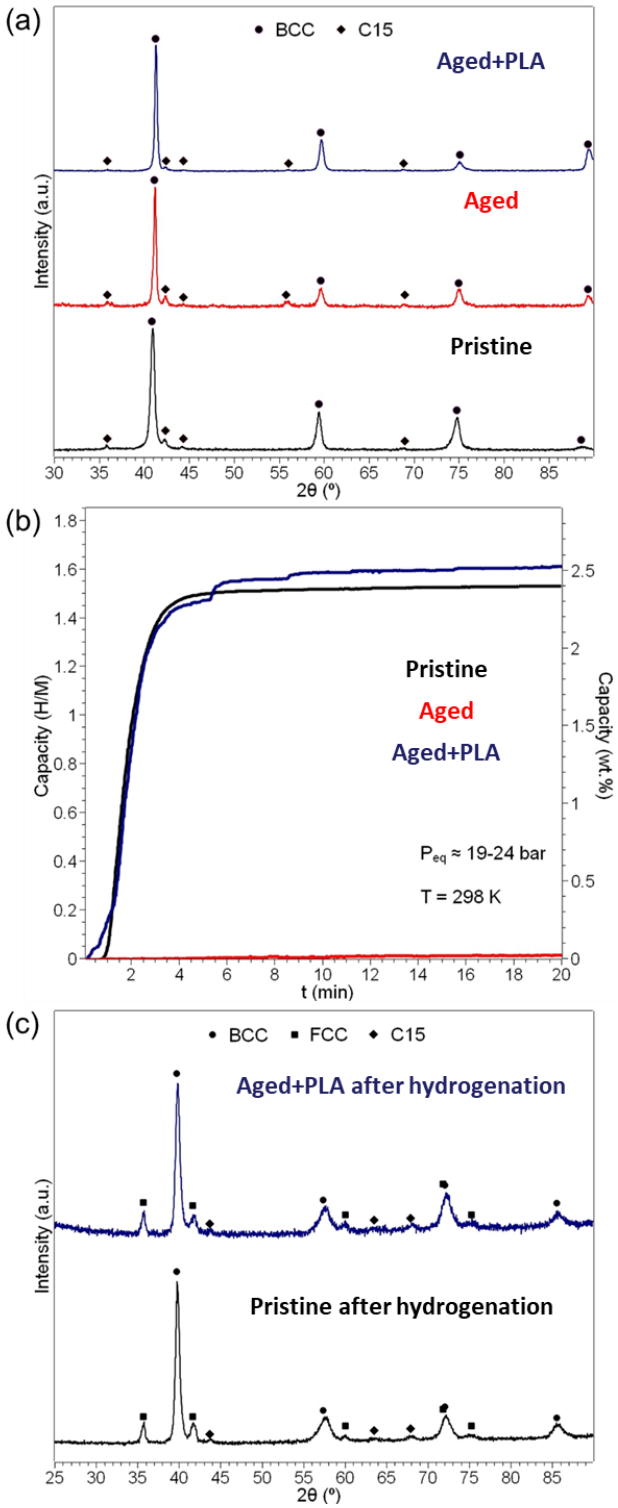

Figure 2: (a) XRD patterns of the pristine, aged, and aged+PLA samples (b) kinetics measurements of the pristine, aged, and aged+PLA samples (c) XRD patterns of the pristine and aged+PLA samples after hydrogenation.

Given that the PLA treatment was able to restore the hydrogen storage ability of the $Ti_{11}V_{30}Nb_{28}Cr_{31}$ alloy without causing significant change of the crystalline phases

structures, we decided to perform further structural analyses in the samples via SEM. Figure 3 shows the Scanning Electron Microscopy (SEM) analyses performed in the pristine and aged+PLA samples before and after hydrogenation. First, it is important to mention that the manual fragmentation process performed in this work produced a random distribution of particle sizes as illustrated in Figures 3 (a), (d), (g) and (j). Therefore, we had limited control regarding this aspect and our discussions will be mainly focused on the particles surface modifications due to the laser activation and/or hydrogenation. Figures 3 (b) and (c) show that the fragmentation of the pristine alloy produced particles with flat surfaces and sharp edges, which were expected given the brittle behavior of the alloy. Figures 3 (e) and (f) demonstrate that the laser treatment clearly modified the surfaces of the particles. The round surfaces/edges of the particles indicate remelting and rapid solidification. The inset on figure 3 (f) shows that the remelted surface has several microcracks that might be beneficial for the sample activation. The remelted surfaces of the particles might have restored the hydrogenation ability of the aged sample. Furthermore, Figures 3 (h), (i), (k) and (l) indicate similar behavior of the samples (pristine and aged+PLA) upon hydrogenation. Surface cracks produced from the volume expansion during hydrogenation were identified in the particles analyzed from both conditions.

Lastly, to obtain a complementary investigation of surface modifications in the analyzed samples, we investigated oxide formation of the samples via XPS analyses. The XPS results displayed in Figure 4 demonstrate that the surface of the aged sample (Figure 4 (b)) closely resembles the pristine sample (Figure 4 (a)). The Nb3d, Ti2p, Cr2p, and V2p spectra in both samples exhibit XPS peaks and components at the same energy levels, indicating the presence of similar surface species. However, notable differences are observed in the aged sample, particularly a higher concentration of metal oxide on its surface compared to the pristine sample. The aged sample shows an atomic concentration of 28 at.% Nb^0 and 72 at.% Nb^{5+}, while the Ti2p spectrum exhibits 15 at.% Ti^0 and 85 at.% Ti^{4+} concentration. Similarly, the Cr2p spectrum displays 15 at.% Cr^0 and 85 at.% Cr^{2+} concentration. In the V2p spectra for the pristine and aged samples, the $V2p_{3/2}$ peak displays a smaller full width at half maximum than the $V2p_{1/2}$ peak due to the Coster–Kronig effect. As a result, precise deconvolution of the peaks becomes challenging. Nevertheless, the presence of V^0 at the energy of 511.8 eV and V^{5+} at the energy of 516.7 eV can be identified. Moreover, it is evident that the intensity of the V^0 peaks decreases,

while the V^{5+} peak increases in the aged sample, following the same trend as observed for the other metals in the alloy. This further supports the indication of increased metal oxide concentration on the aged sample surface compared to the pristine sample. Overall, these findings suggest that while the surface species in the aged sample remain similar to the pristine sample, there is an increased proportion of metal oxide species, notably Nb^{5+}, Ti^{4+}, Cr^{2+} and V^{5+} indicating the influence of aging on the alloy's surface composition.

In Figure 4 (c), the XPS results for the aged+PLA sample are presented. In contrast to the results obtained for the pristine and aged samples, the $Ti_{11}V_{30}Nb_{28}Cr_{31}$ alloy after undergoing laser treatment, exhibits only metal oxide species on its surface, specifically Nb^{5+}, Ti^{4+}, Cr^{2+}, and V^{5+}. No components associated with pure metals were observed, indicating complete oxidation of the surface after the laser processing. It is worth mentioning that all the experiments (sample aging and XPS measurements) reported here were carried out at least twice and the results presented very good reproducibility.

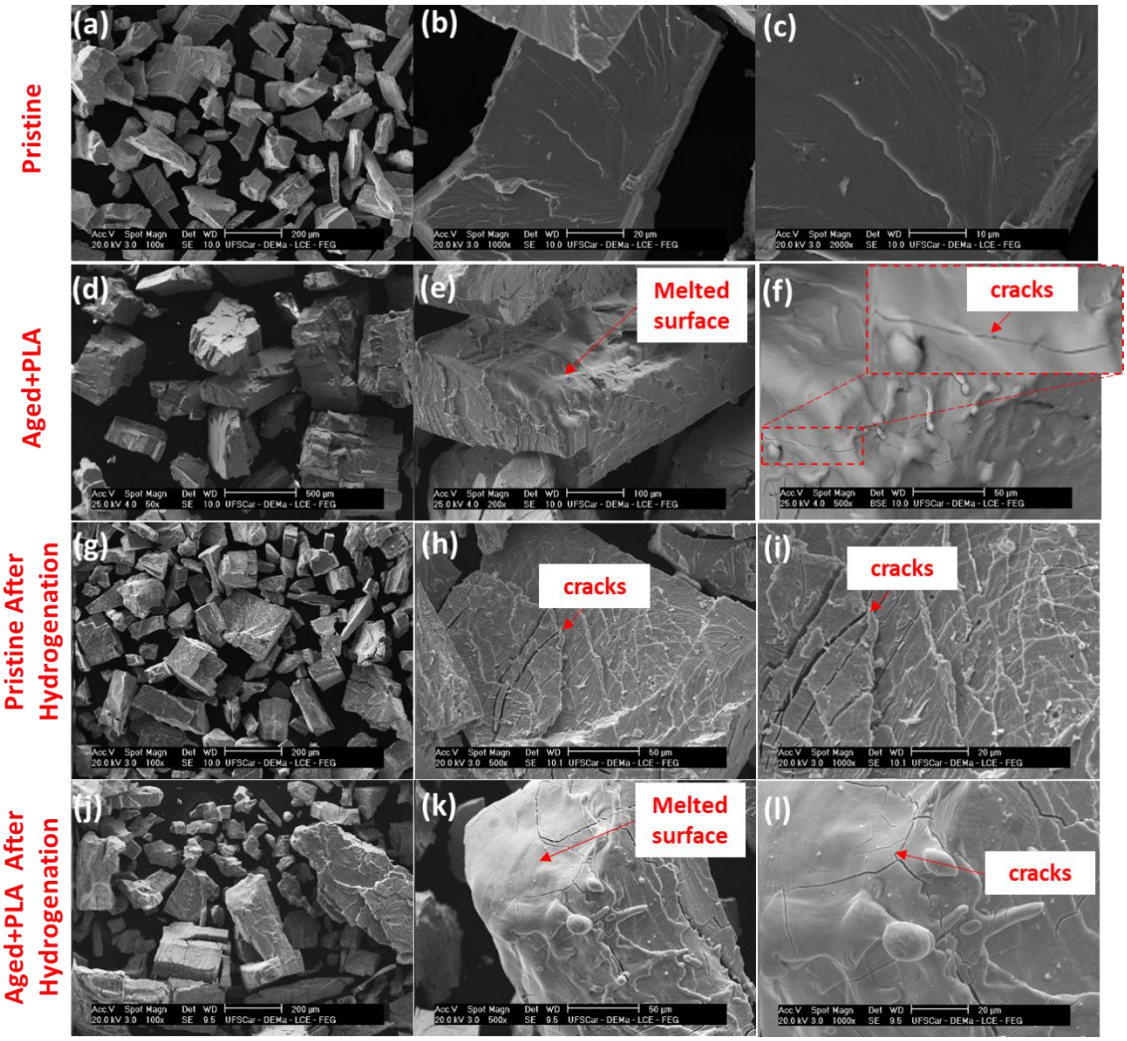

Figure 3: SEM analyses of the (a), (b), and (c) pristine sample; (d), (e), and (f) aged+PLA sample; (g), (h), and (i) pristine sample after hydrogenation; and (j), (k), and (l) aged+PLA sample after hydrogenation.

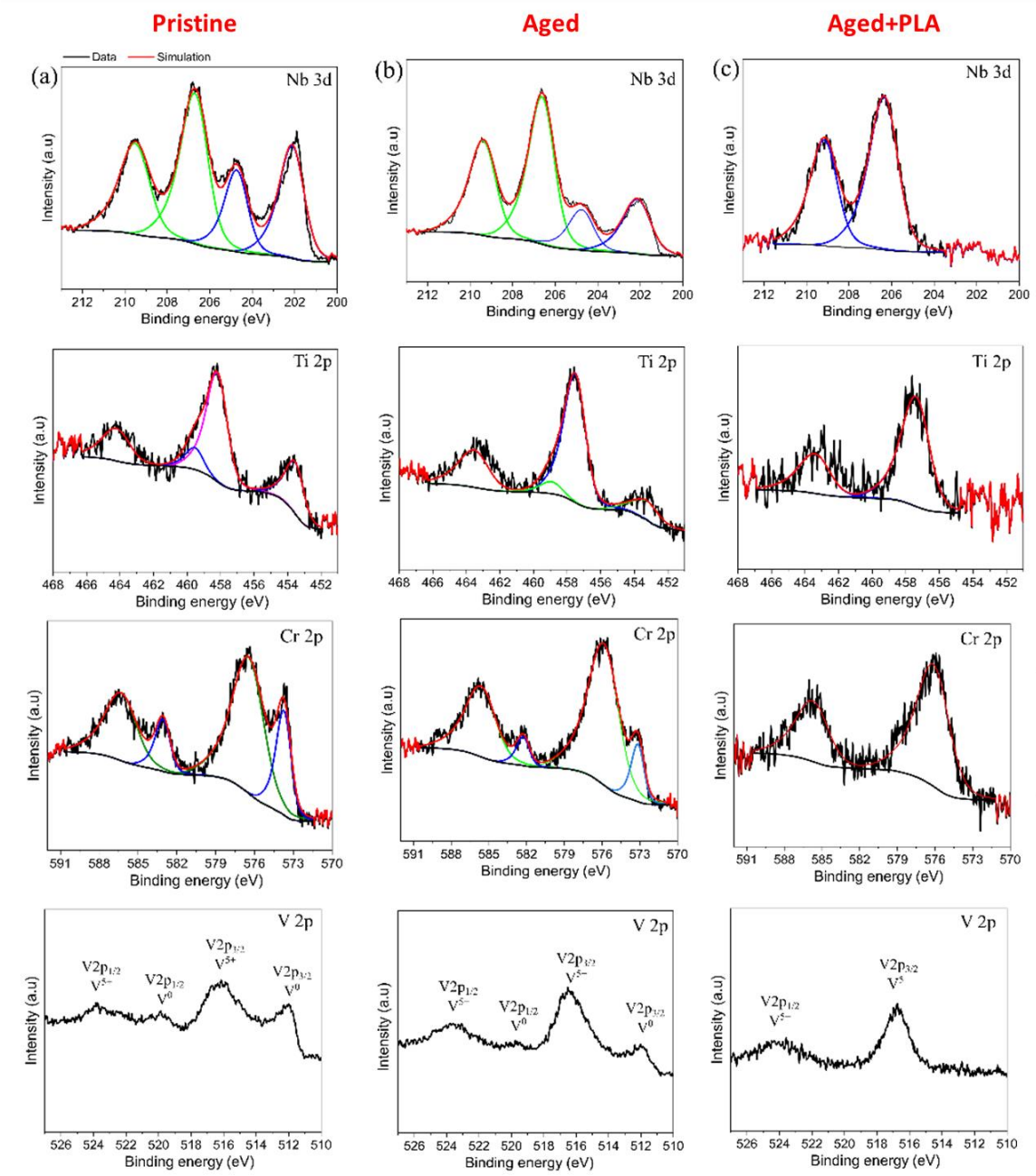

Figure 4: High-resolution Nb, Ti, Cr, and V XPS spectra of (a) the pristine sample, (b) the aged sample, and (c) the aged+LA sample.

At first glance, these results may appear controversial since one would expect the XPS spectra of the aged+PLA samples to exhibit behavior similar to that of the pristine

samples. Nanosecond laser processing induces rapid and significant surface alterations. In our experiments, we were able to trace the changes that occurred on the alloy surfaces from ablation to melting, all within the confines of the laser plume. Consequently, the metallic alloy's surface becomes considerably more reactive to oxygen in the ambient atmosphere, resulting in the formation of a thicker oxide layer, as evidenced by the XPS spectra. A. Santhosh et al. [26] reported a comprehensive investigation on the effect of the near-surface oxide layers on the hydrogenation of TiFe, which is an intermetallic compound known for its difficult activation. Their results show that the type, orientation, and composition of the oxides formed on the alloy's surface play important roles in the hydrogen diffusion path. One insight regarding the effect of oxides on the activation of TiFe reported by the authors is that different types of oxides can be formed on the TiFe surface (for instance, TiO_2, $TiFeO_3$, $Ti(FeO_2)_2$, and Ti_2FeO_5). The different types of oxides may expand differently from each other generating cracks that can facilitate the H transport from the surface to the bulk. This hypothesis has also been discussed by other authors [34].

The SEM analyses of the aged+PLA sample clearly show that the alloy surface was melted during laser processing. It was also possible to verify the presence of cracks on the surface, shown in Figure 3 (f). Because of the multicomponent characteristic of the alloys, different oxides could be formed on the alloy surface, which corroborates with the different valence of the metallic cations measured by XPS (Nb^{5+}, Ti^{4+}, Cr^{2+}, and V^{5+}). The different oxides with different expansion coefficients could lead to cracks on the near-surface oxide layer, which might be responsible for the activation. However, one must consider that the activation process of alloys for hydrogen storage is a complex phenomenon, and its mechanisms are not completely understood yet. Nevertheless, it is important to emphasize again the effectiveness of the PLA treatment for the $Ti_{11}V_{30}Nb_{28}Cr_{31}$ alloy. This activation treatment seems very promising, especially for large scale applications of metal hydrides, and we hope that the insights provided in this work can inspire new developments in this area.

4. Conclusions

We introduced for the first time the concept of Pulsed Laser Activation for hydrogen storage alloys. We demonstrated that the hydrogen storage ability of the 30 days air exposed $Ti_{11}V_{30}Nb_{28}Cr_{31}$ alloy can be completely restored by scanning the fragmented sample with a nanosecond pulsed laser for only three minutes (scan speed of 400

mm/min). Although the laser activation mechanism of the $Ti_{11}V_{30}Nb_{28}Cr_{31}$ alloy was not completely understood yet, we showed that during laser processing the surface of the fragmented particles are melted and that the fraction of oxides near to the surface is increased. The PLA is a novel and innovative method for restoring the hydrogen storage ability of air-exposed BCC alloys. This method can be easily transferred to other alloys and intermetallic compounds, and it is a promising alternative for fast and easy activation (or re-activation) of alloys applied to solid-state hydrogen storage tanks.

Acknowledgments

This work was financed in part by the Serrapilheira Institute (grant number Serra-1709–17362) and in part by the Brazilian National Council for Scientific and Technological Development – CNPq (Grant numbers: 309467/2021-7, 312235/2021-6). This study was also financed in part by the Coordenação de Aperfeiçoamento de Pessoal de Nível Superior - Brasil (CAPES) - Finance Code 001, Federal University of Sao Carlos, Graduate Program in Materials Science and Engineering. The authors are grateful to the Laboratory of Structural Characterization (LCE/DEMa/UFSCar) for the electron microscopy and X-ray diffraction facilities.

References

[1] A. Züttel, Materials Today 6 (2003) 24–33.

[2] F. Marques, M. Balcerzak, F. Winkelmann, G. Zepon, M. Felderhoff, Energy Environ Sci (2021).

[3] D. Karlsson, G. Ek, J. Cedervall, C. Zlotea, K.T. Møller, T.C. Hansen, J. Bednarčík, M. Paskevicius, M.H. Sørby, T.R. Jensen, U. Jansson, M. Sahlberg, Inorg Chem 57 (2018) 2103–2110.

[4] G. Ek, M.M. Nygård, A.F. Pavan, J. Montero, P.F. Henry, M.H. Sørby, M. Witman, V. Stavila, C. Zlotea, B.C. Hauback, M. Sahlberg, Inorg Chem 60 (2021) 1124–1132.

[5] C. Zlotea, M.A. Sow, G. Ek, J.-P. Couzinié, L. Perrière, I. Guillot, J. Bourgon, K.T. Møller, T.R. Jensen, E. Akiba, M. Sahlberg, J Alloys Compd 775 (2018) 667–674.

[6] M.M. Nygård, G. Ek, D. Karlsson, M.H. Sørby, M. Sahlberg, B.C. Hauback, Acta Mater 175 (2019) 121–129.

[7] J. Montero, C. Zlotea, G. Ek, J. Crivello, L. Laversenne, M. Sahlberg, Molecules 24 (2019) 2799.

[8] M. Sahlberg, D. Karlsson, C. Zlotea, U. Jansson, Sci Rep 6 (2016) 36770.

[9] J. Montero, G. Ek, M. Sahlberg, C. Zlotea, Scr Mater 194 (2021) 113699.

[10] R.B. Strozi, D.R. Leiva, J. Huot, W.J. Botta, G. Zepon, Int J Hydrogen Energy 46 (2021) 2351–2361.

[11] G. Zepon, D.R. Leiva, R.B. Strozi, A. Bedoch, S.J.A. Figueroa, T.T. Ishikawa, W.J. Botta, Int J Hydrogen Energy 43 (2018) 1702–1708.

[12] R. Floriano, G. Zepon, K. Edalati, G.L.B.G. Fontana, A. Mohammadi, Z. Ma, H.-W. Li, R.J. Contieri, Int J Hydrogen Energy 45 (2020) 33759–33770.

[13] B.H. Silva, C. Zlotea, Y. Champion, W.J. Botta, G. Zepon, J Alloys Compd 865 (2021) 158767.

[14] P. Edalati, R. Floriano, A. Mohammadi, Y. Li, G. Zepon, H.W. Li, K. Edalati, Scr Mater 178 (2020) 387–390.

[15] J. Montero, G. Ek, L. Laversenne, V. Nassif, G. Zepon, M. Sahlberg, C. Zlotea, J Alloys Compd 835 (2020) 155376.

[16] F. Marques, H.C. Pinto, S.J.A. Figueroa, F. Winkelmann, M. Felderhoff, W.J. Botta, G. Zepon, Int J Hydrogen Energy 45 (2020) 19539–19552.

[17] M.M. Nygård, Ø.S. Fjellvåg, M.H. Sørby, K. Sakaki, K. Ikeda, J. Armstrong, P. Vajeeston, W.A. Sławiński, H. Kim, A. Machida, Y. Nakamura, B.C. Hauback, Acta Mater 205 (2021).

[18] R.B. Strozi, B.H. Silva, D.R. Leiva, C. Zlotea, W.J. Botta, G. Zepon, J Alloys Compd 932 (2023) 167609.

[19] S. Suwarno, J.K. Solberg, J.P. Maehlen, B. Krogh, V.A. Yartys, Int J Hydrogen Energy 37 (2012) 7624–7628.

[20] S.W. Cho, C.S. Han, C.N. Park, E. Akiba, J Alloys Compd 288 (1999) 294–298.

[21] T. Tamura, T. Kazumi, A. Kamegawa, H. Takamura, M. Okada, J Alloys Compd 356–357 (2003) 505–509.

[22] H. Arashima, F. Takahashi, T. Ebisawa, H. Itoh, T. Kabutomori, J Alloys Compd 356–357 (2003) 405–408.

[23] T. Kuriiwa, T. Maruyama, A. Kamegawa, M. Okada, Int J Hydrogen Energy 35 (2010) 9082–9087.

[24] H. Itoh, H. Arashima, K. Kubo, T. Kabutomori, K. Ohnishi, J Alloys Compd 404–406 (2005) 417–420.

[25] B. Hessel Silva, W.J. Botta, G. Zepon, Int J Hydrogen Energy (2023).

[26] A. Santhosh, S. Kang, N. Keilbart, B.C. Wood, T. Klassen, P. Jerabek, M. Dornheim, J Mater Chem A Mater (2023).

[27] H. Liu, J. Zhang, P. Sun, C. Zhou, Y. Liu, Z.Z. Fang, Int J Hydrogen Energy (2023) 1–14.

[28] A.K. Patel, D. Siemiaszko, J. Dworecka-Wójcik, M. Polański, Int J Hydrogen Energy 47 (2022) 5361–5371.

[29] S.N.C. Santos, J.M.P. Almeida, G.F.B. Almeida, V.R. Mastelaro, C.R. Mendonca, Opt Commun 427 (2018) 33–36.

[30] R.G. Capelo, J.M.P. Almeida, D.F. Franco, G.Y. Poirier, C.R. Mendonça, M. Nalin, D. Manzani, Journal of Materials Research and Technology 13 (2021) 1296–1304.

[31] M. V. Santos, S.N.C. Santos, R.J. Martins, J.M.P. Almeida, K.T. Paula, G.F.B. Almeida, S.J.L. Ribeiro, C.R. Mendonça, Journal of Materials Science: Materials in Electronics 30 (2019) 16843–16848.

[32] J.M.P. Almeida, G.F.B. Almeida, A.C. Hernandes, C.R. Mendonça, CrystEngComm 18 (2016) 5959–5964.

[33] C. Oncebay, J.M.P. Almeida, G.F.B. Almeida, S.R. Muniz, C.R. Mendonca, Diam Relat Mater 130 (2022) 109426.

[34] D.M. Dreistadt, L. Thi-Thu, G. Capurso, J.M. Bellosta von Colbe, A. Santhosh, C. Pistidda, N. Scharnagl, H. Ovri, C. Milanese, P. Jerabek, T. Klassen, J. Jepsen, J Alloys Compd 919 (2022) 165847.